

Sonoanatomy of the Major Salivary Glands

9

Sandrine Jousse-Joulin and George A. W. Bruyn

Introduction

Anatomical knowledge of the major salivary glands (MSG) is key for a correct assessment of ultrasound images. As to a detailed description of their anatomy, the reader is referred to the previous chapter.

Embryology

During foetal development, the parotid gland anlagen are the first to appear, followed by the anlagen of the submandibular glands and the sublingual glands. The minor salivary glands do not start to develop until much later. Although the parotid gland anlagen are the first to develop, they only become encapsulated after the submandibular and sublingual glands. The period between the encapsulation of the submandibular and sublingual glands and the parotid gland encapsulation is characterised by the development of the lymphatic system in the mesoderm. As a result, intraglandular lymph nodes and lymphatic channels are present inside the parotid glands of adults, but not in the submandibular and sublingual glands. Therefore, the presence of lymph nodes within the parotid glands is considered a normal finding whereas it is not in the other glands [1, 2]. The relationship of the parotid gland to the extratemporal facial nerve, i.e., when the facial nerve exits the stylomastoid foramen, is also prone to change in the first years of life. In the adult, the facial nerve is protected on the lateral side by the tip of the mastoid, the tympanic ring, and the mandibular ramus, while in children younger than 2 years the trunk of the nerve runs a subcutaneous course.

S. Jousse-Joulin (✉)
 CHU de Brest, Univ Brest, Inserm, LBAI, UMR1227,
 Brest, France
 e-mail: sandrine.jousse-joulin@chu-brest.fr

G. A. W. Bruyn
 Reumakliniek Lelystad, Lelystad, The Netherlands

Ultrasound Examination of the Major Salivary Glands

Parotid Glands

Both parotids are examined in both longitudinal or coronal and transverse or axial planes. The parotid gland may be assessed in a transverse plane perpendicular to the ascending ramus of the mandible and using the condyle of the temporomandibular joint as a landmark (Fig. 9.1). In the longitudinal plane, the probe is positioned parallel to the ascending ramus of the mandible (Fig. 9.2).



Fig. 9.1 Position of the probe for parotid gland scanning-longitudinal or coronal scan

Sonographic Appearance of the Parotid Gland

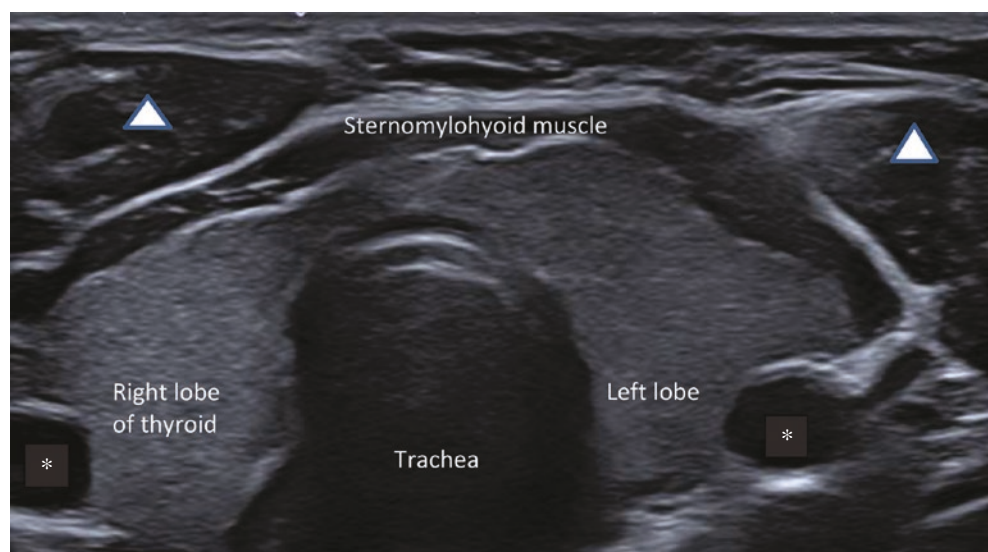
The parotid gland is scanned in two axes, i.e., coronal or longitudinal, and axial or transverse, parallel to the mandibular bone (Figs. 9.1 and 9.2). The major salivary glands must be compared to the homogeneous thyroid parenchyma (Fig. 9.3) and in healthy persons, the homogeneous gland structure provides a clear demarcation from the superficial tissue and increased echogenicity relative to adjacent muscle (Figs. 9.3 and 9.4).

The parotid gland is divided into two lobes by vessels (retromandibular vein and external carotid artery) defining a superficial and a deep lobe. These vessels should be used as a



Fig. 9.2 Position of the probe for parotid gland scanning-axial or transverse scan

Fig. 9.3 Axial (transverse) scan of the thyroid demonstrating a homogeneous echogenic thyroid tissue. Asterisks indicate carotid arteries. Pyramids indicate sternocleidomastoid muscles



landmark to separate the superficial lobe from the deep lobe. The larger superficial lobe is clearly visible using a linear array 18–12 MHz probe. The superficial lobe may contain lymph nodes, i.e., one in the upper, and/or one in the middle, and/or one in the lower pole of the gland (Fig. 9.5). Normal intraparotid lymph nodes commonly demonstrate an ovoid shape. The presence of a fatty, hyperechoic hilum is one of the characteristics of a benign parotid lymph node (Fig. 9.5). With the application of sensitive power Doppler US, central vessels may be seen in normal parotid lymph nodes.

The smaller deep lobe of the parotid gland is difficult to assess. For the evaluation of the deeper lobe, the frequency should be lowered to around 10 Mhz.

Penetration of the ultrasound beam into the deep lobe of the parotid gland is hindered by the high fat content of the parenchyma. As a result, significant attenuation of the sound waves occurs, increasing the echogenicity of the parenchyma and blurring the contours of the gland. Unless in a dilated condition, the excretory duct (Stensen's duct) is not visible except in slim individuals.

The parotid gland is vascularised by the external carotid artery and retromandibular vein which are given landmarks for distinguishing the deep from the superficial lobe. Commonly these vessels are identified by Doppler ultrasound, but sometimes they can also be imaged in B mode.

After exiting the stylomastoid foramen, the facial nerve can be partly visualised in the posterior part of the gland, where the trunk runs superficial to the main intraparotid vessels.

Submandibular Gland

The submandibular glands are lying in the submandibular triangle, whose margins are formed by the anterior and pos-

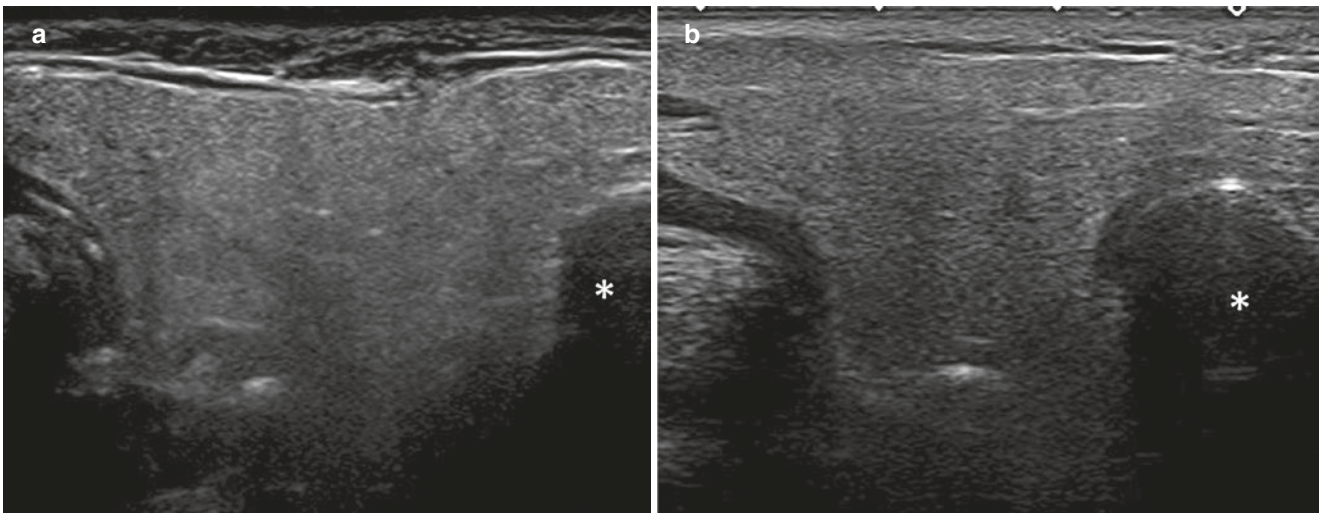
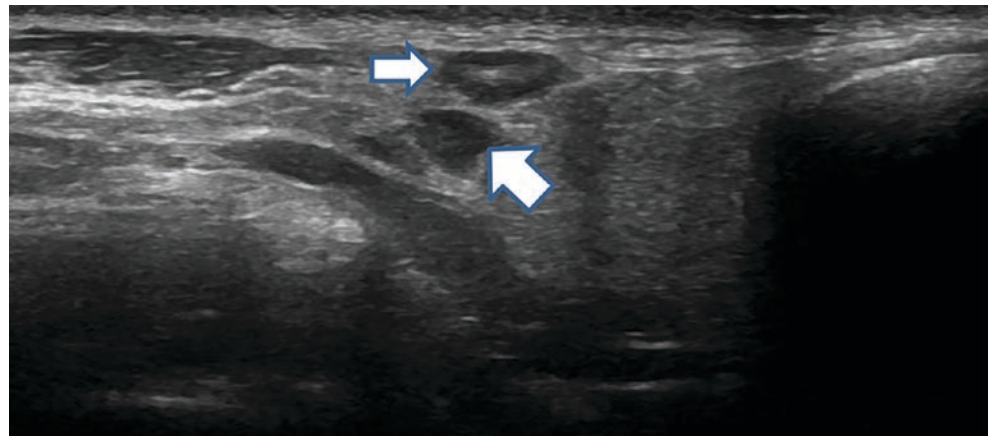


Fig. 9.4 Ultrasound of the parotid gland. (a) Coronal or longitudinal scan of the parotid gland. Left side of the image is cranial, right is caudal. Star indicates the mandibular bone. (b) Axial or transverse scan of

the parotid gland. Left side of the image is posterior, showing the mastoid bone and the transverse artery coursing on top, and right side is the mandible

Fig. 9.5 Axial scan of the parotid gland showing two lymph nodes in the superficial lobe. The upper lymph node clearly demonstrates a hyperechoic hylum



terior bellies of the digastric muscle and the inferior border of the mandible.

The submandibular glands are assessed in longitudinal and transverse planes in the posterior part of the submandibular triangle with the posterior belly of digastric muscle as a landmark. In some cases, the submandibular gland may be connected with the parotid gland by the stylomandibular ligament. The longitudinal and transverse scanning planes are conversely defined in comparison to the parotid planes. For reliability reasons, the OMERACT protocol recommends assessing the submandibular gland only in longitudinal or coronal planes (Figs. 9.6 and 9.7).

Sonographic Appearance of the Submandibular Gland

In healthy individuals, the submandibular gland sonoanatomy using a linear array 18–12 MHz probe shows an almost

perfect homogeneous gland tissue similar to the thyroid gland, with a clear delineation from the superficial tissue and increased echogenicity relative to adjacent muscle. The homogeneous echotexture of the submandibular gland is much better visible than the echotexture of the parotid gland, as it contains less fat and is more cellular (Fig. 9.8).

With the exception of very slim persons, the excretory duct (Wharton's duct) is normally not visible. The submandibular gland is vascularised by the facial artery and vein coming from the external carotid. The facial artery runs across the parenchyma and without excess pressure on the probe readily visible in B mode. The facial vein runs along the anterosuperior part of the submandibular gland and may be visible.

As previously stated, there are no lymph nodes within the parenchyma but they can be found in the anterior part and outside of the gland.



Fig. 9.6 Probe position for submandibular gland scanning-longitudinal or coronal scan



Fig. 9.7 Position of the probe for submandibular gland scanning-transverse or axial scan

Sublingual Gland

The sublingual glands are the smallest of the major salivary glands and are lying in the submental triangle, where they can be imaged by ultrasound. These glands are lying above the mylohyoid and lateral to the genioglossus muscle (Fig. 9.9).

Normal sublingual gland parenchyma has a uniformly hyperechoic texture compared to adjacent muscles, and echotexture of the gland is comparable to the thyroid parenchyma. The sublingual glands should be assessed in coronal or transverse planes.

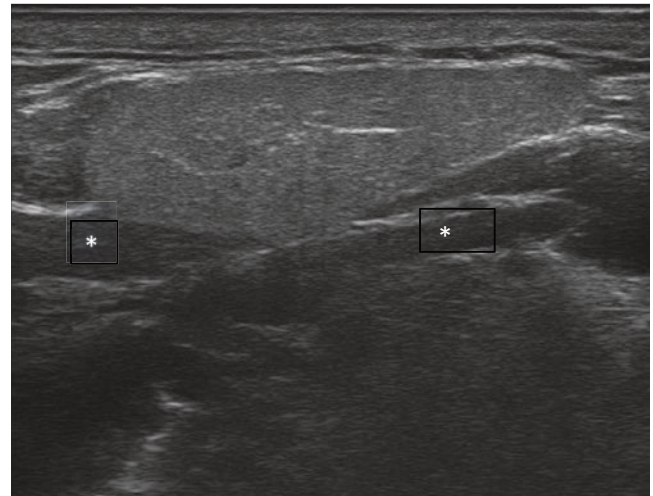


Fig. 9.8 Longitudinal or coronal scan of the submandibular gland. Note the similarity of the echotexture to that of the thyroid. Asterisks indicate the anterior and posterior bellies of the digastric muscle

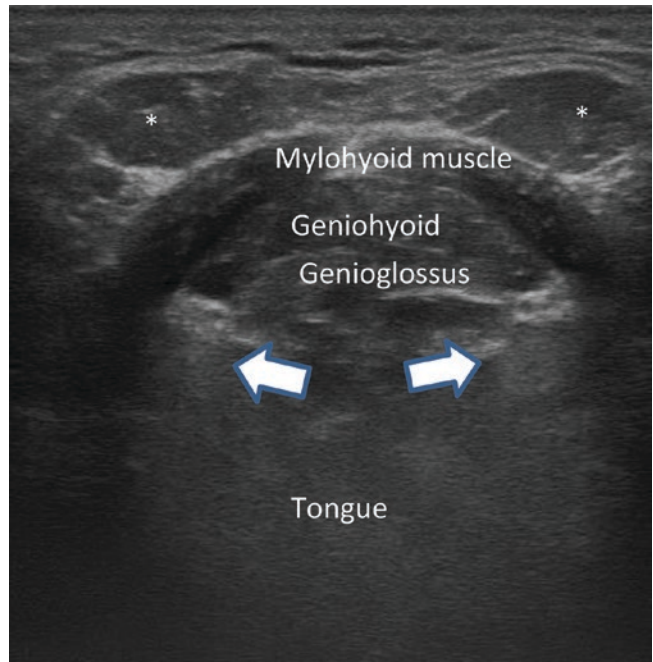


Fig. 9.9 Coronal scan through the submental space. Star indicates anterior belly of digastric muscle. Asterisks indicate the anterior belly of digastric muscle; arrows point to sublingual glands with visible salivary ducts

Sonographic Appearance of the Sublingual Gland

In the coronal plane, the sublingual glands are ovoidly shaped (Figs. 9.9 and 9.10). In a longitudinal plane parallel to the inferior border of the mandible, the shape is lentiform. Since the size of the sublingual glands is small, the OMERACT scoring system for Sjögren's syndrome does not include these glands.



Fig. 9.10 Coronal scan plane for sublingual glands

The glands have no clear demarcation from the adjacent tissues because they lack a true fascial capsule (Fig. 9.9). The sublingual glands are drained by approximately 10 small ducts which can be visualised by ultrasound on the medial side of the glands. Since the sublingual glands are difficult to visualise by ultrasound, MRI is the superior method of imaging.

Salivary Gland Abnormalities in Primary Sjögren Syndrome

Greyscale ultrasound has traditionally been used to differentiate solid from cystic salivary gland masses and to identify salivary calculi. Other benefits of ultrasound are the identification of the more advanced stages of gland lesions in autoimmune disease, including Sjögren's syndrome. The sonographic gland lesion of Sjögren syndrome is typically a mottled parenchymal heterogeneity consisting of widespread an- or hypoechoic areas [3–18].

Based on the extent of these an- and hypoechoic areas, various authors have proposed a semiquantitative scoring system to stage the degree of MSG involvement. As an example, the OMERACT 4-grade semiquantitative score is illustrated in Fig. 9.11 [5]. The greyscale ultrasound lesions correspond to different histological changes occurring during the pro-

gressive stages of the disease. The hypoechoic areas that are responsible for the heterogeneity of the parenchyma of the glands are due either to an infiltration of the gland by inflammatory cells or to fat depositions within the gland. In other words, the an- or hypoechoic areas also called “pseudocysts” correspond to the ectasia of the lobular salivary ducts secondary to the inflammatory infiltrate; their number and size are proportional to the extent of lesions observed on standard sialography or MRI sialography [16, 19–22]. Over time, these pseudocysts may reveal, although not consistently, small punctiform aggregates [23]. In addition to these four stages, a late-stage disease gland, i.e., a fibrotic salivary gland, can develop after a considerable amount of time, characterised by hyperechoic bands and increased echogenicity, resulting in difficulties to distinguish the gland from the adjacent tissue. In late-stage Sjögren disease, the salivary glands become destroyed, showing a diffuse adipose infiltration. This fatty infiltration accounts for the disappearance of gland borders on ultrasound assessment. In addition to the disappearance of the gland demarcation, ultrasound shows a gland parenchyma characterised by the hyperechoic bands secondary to postinflammatory fibrosis [8].

Different stages of the disease may coexist at the same time in the various salivary glands in the same patient. Our recommendation therefore is always to assess the four major salivary glands and not just one side (one unilateral PG and one SMG) in routine care. Involvement of a single gland should lead to discussing a differential diagnosis.

Ultrasound Technique for Major Salivary Glands Assessment

Machine Assessing the major salivary glands requires the use of an ultrasound machine with a 10–18 Mhz linear probe. Each patient is scanned in the supine position with the neck hyperextended and the head turned to the opposite side. As a preferred presetting of the machine sensitivity, the gland parenchyma is compared to the thyroid gland because the two glands are very similar in echostructure.

The greyscale mode provides echostructural details. The vascularization of the glands should be evaluated by using Doppler colour [24] Elastography studies are rare and have yet to show their added value in the context of Sjögren's syndrome [25]. For a superior evaluation of the facial nerve, a 22 MHZ probe is preferred, which is able to show the main trunk.

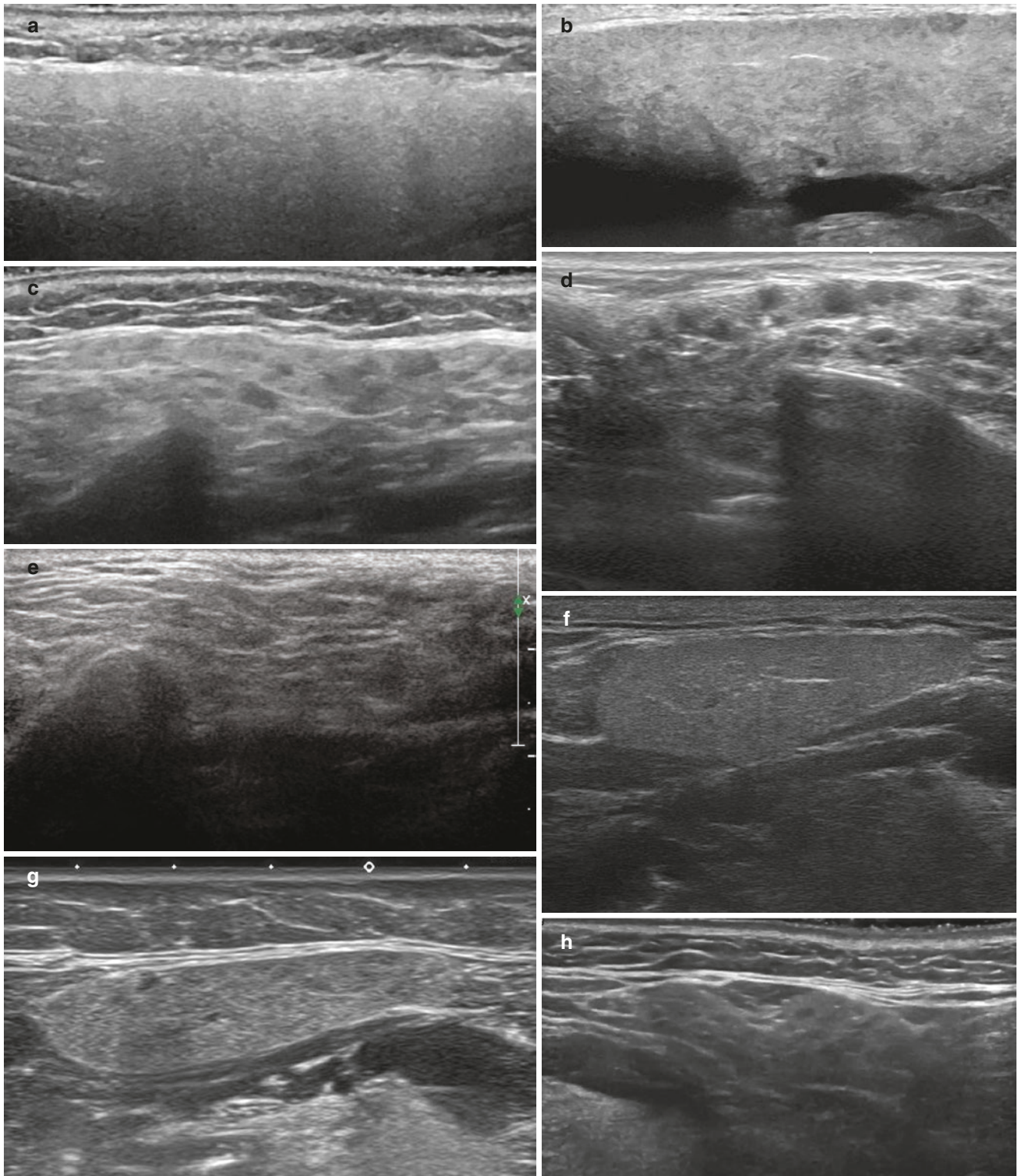


Fig. 9.11 The OMERACT 4-grade semiquantitative ultrasound score for major salivary glands (a–j). (a) Grade 0, normal echotexture of parotid gland. (b) Grade 1, mild inhomogeneous echotexture of parotid gland, no hypoechoic lesions and no hyperechoic bands. (c) Grade 2, moderate inhomogeneous echotexture with focal hypoechoic lesions, no hyperechoic bands. (d) Grade 3, severe inhomogeneous echotexture showing widespread hypoechoic lesions and scarce fibrotic bands in the

parotid gland. (e) Grade 3, fibrous parotid gland, with no discernible gland borders. (f) Grade 0, normal echotexture of submandibular gland. (g) Grade 1, mild inhomogeneous echotexture without hypoechoic lesions. (h) Grade 2, moderate inhomogeneous echotexture with focal hypoechoic lesions. (i) Grade 3, severe inhomogeneous echotexture with wide spread hypoechoic lesions. (j) Grade 3, fibrous submandibular gland

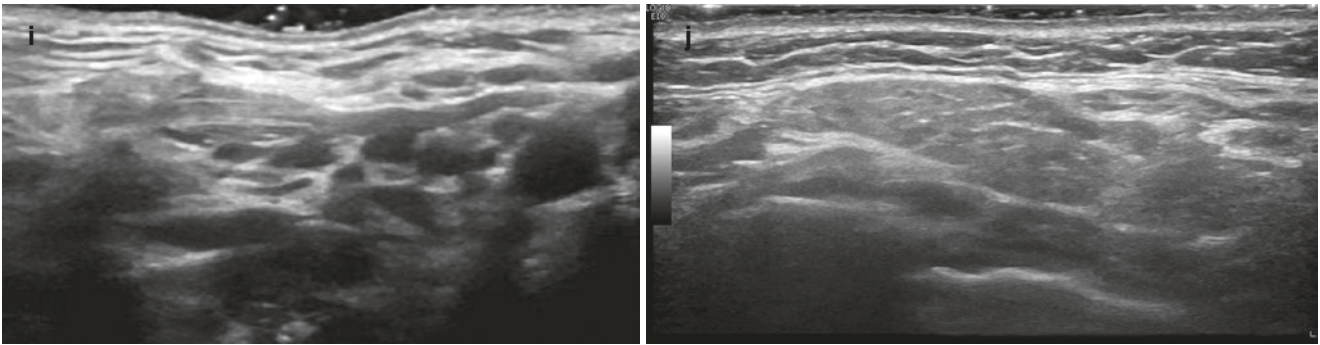


Fig. 9.11 (continued)

References

- Silvers AR, Som PM. Salivary glands. *Radiol Clin N Am*. 1998;36(5):941–66.
- Beale T, Madani G. Anatomy of the salivary glands. *Semin Ultrasound CT MR*. 2006;27(6):436–9.
- De Vita S, Lorenzon G, Rossi G, et al. Salivary gland echography in primary and secondary Sjögren's syndrome. *Clin Exp Rheumatol*. 1992;10:351–6.
- Ariji Y, Ohki M, Eguchi K, et al. Texture analysis of sonographic features of the parotid gland in Sjögren's syndrome. *AJR*. 1996;166:935–41.
- Jousse-Joulin S, et al. Video clip assessment of a salivary gland ultrasound scoring system in Sjögren's syndrome using consensual definitions: an OMERACT ultrasound working group reliability exercise. *Ann Rheum Dis*. 2019;78(7):967–73.
- Clerck D, et al. Ultrasonography and computer tomography of the salivary glands in the evaluation of Sjögren's syndrome. Comparison with parotid sialography. *J Rheumatol*. 1988;15:1777–81.
- Makula E, et al. Parotid gland ultrasonography as a diagnostic tool in primary Sjögren's syndrome. *Br J Rheumatol*. 1996;35:972–7.
- Salaffi F, et al. Salivary gland ultrasonography in the evaluation of primary Sjögren's syndrome. Comparison with minor salivary gland biopsy. *J Rheumatol*. 2000;27(5):1229–36.
- Yonetsu K, et al. Sonography as a replacement for sialography for the diagnosis of salivary glands affected by Sjögren's syndrome. *Ann Rheum Dis*. 2002;61:276_7.
- El Miedany YM, et al. Quantitative ultrasonography and magnetic resonance imaging of the parotid gland: can they replace the histopathologic studies in patients with Sjögren's syndrome? *Joint Bone Spine*. 2004;71:29–38.
- Hocevar A, et al. Ultrasonographic changes of major salivary glands in primary Sjögren's syndrome. Diagnostic value of a novel scoring system. *Rheumatology*. 2005;44:768–72.
- Shimizu M, et al. Sonographic diagnosis of Sjögren syndrome: evaluation of parotid gland vascularity as a diagnostic tool. *Oral Surg Oral Med Oral Pathol Oral Radiol Endod*. 2008;106:587–94.
- Chikui T, et al. Quantitative analyses of sonographic images of the parotid gland in patients with Sjögren's syndrome. *Ultrasound Med Biol*. 2006;32:617–22.
- Wernicke D, et al. Ultrasonography of salivary glands -a highly specific imaging procedure for diagnosis of Sjögren's syndrome. *J Rheumatol*. 2008;35:285–93.
- Poul JH, et al. Retrospective study of the effectiveness of high-resolution ultrasound compared with sialography in the diagnosis of Sjögren's syndrome. *Dentomaxillofac Radiol*. 2008;37:392–7.
- Salaffi F, et al. Ultrasonography of salivary glands in primary Sjögren's syndrome: a comparison with contrast sialography and scintigraphy. *Rheumatology*. 2008;47(8):1244–9.
- Milic V, et al. Ultrasonography of major salivary glands could be an alternative tool to sialoscintigraphy in the American-European classification criteria for primary Sjögren's syndrome. *Rheumatology*. 2012;51:1081–5.
- Milic VD, et al. Major salivary gland sonography in Sjögren's syndrome: diagnostic value of a novel ultrasonography score (0-12) for parenchymal inhomogeneity. *Scand J Rheumatol*. 2010;39:160–6.
- Jousse-Joulin S, et al. Salivary gland ultrasound abnormalities in primary Sjögren's syndrome: consensual US-SG core items definition and reliability. *RMD Open*. 2017;3(1):e000364.
- Niemela RK, et al. Ultrasonography of salivary glands in primary Sjögren's syndrome. A comparison with magnetic resonance imaging and magnetic resonance sialography of parotid glands. *Rheumatology*. 2004;43(7):875–9.
- Yonetsu K, et al. Sonography as a replacement for sialography for the diagnosis of salivary glands affected by Sjögren's syndrome. *Ann Rheum Dis*. 2002;61(3):276–7.
- Song GG, Lee YH. Diagnostic accuracies of sialography and salivary ultrasonography in Sjögren's syndrome patients: a meta-analysis. *Clin Exp Rheumatol*. 2014;32(4):516e22.
- De Vita S, et al. Salivary gland echography in primary and secondary Sjögren's syndrome. *Clin Exp Rheumatol*. 1992;10:351–6.
- Hocevar A, et al. Assessing the vascularization of salivary glands in patients with Sjögren's syndrome - the OMERACT US sub-task group reliability exercise. *Arthritis Rheum* 2019;71(suppl 10) [abstract]. <https://acrabstracts.org/abstract/assessing-the-vascularization-of-salivary-glands-in-patients-with-sjogrens-syndrome-anomeract-ultrasound-group-reliability-exercise/>.
- Samier-Guérin A, et al. Can ARFI elastometry of the salivary glands contribute to the diagnosis of Sjögren's syndrome? *Joint Bone Spine*. 2016;83(3):301–6.